LBL-2945

Presented at the International
Conference on Reactions Between
Complex Nuclei, Nashville, Tennessee,
June 10-14, 1974

MACROSCOPIC ASPECTS OF HEAVY-ION REACTIONS

William D. Myers

June 1974

Prepared for the U. S. Atomic Energy Commission
under Contract W-7405-ENG-48

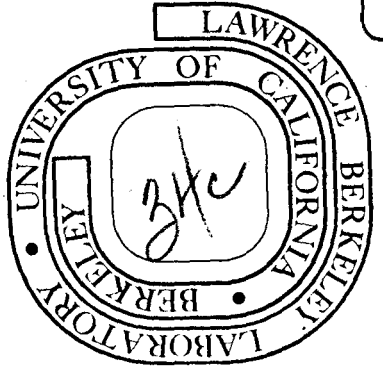

LBL-2945

DISCLAIMER

MACROSCOPIC ASPECTS OF HEAVY-ION REACTIONS*

William D. Myers

Lawrence Berkeley Laboratory
University of California
Berkeley, California 94720

June 1974

CONTENTS

*Work performed under the auspices of the U. S. Atomic Energy Commission.

I. INTRODUCTION

The macroscopic approach, which has made so many contributions to our understanding of nuclear fission, nuclear masses and various types of collective nuclear properties, is now being applied to heavy-ion reactions. The rate at which publications employing this approach are appearing in the scientific literature seems to be growing exponentially for a number of different reasons. (For recent reviews see refs. [1-3].) The most important is the increasing experimental interest in these reactions associated with the search for superheavy elements and the availability of new heavy-ion accelerators. Another reason is that, not only is a macroscopic approach possible (because both the target and projectile are composite systems with $A >> 1$), but classical or semi-classical methods are applicable as well (because the "action" $>> \hbar$). The final, and probably the most important, reason for the explosive growth of this field is that it is easy and it is fun.

Much of the work going on is at the relatively primitive stage of trying to establish plausible links between phenomena which actually require a dynamical description (such as compound nucleus formation for a particular target, projectile combination, energy and angular momentum) and some feature of the one dimensional (radial separation) potential energy surface (i.e. does the potential contain a minimum in which the system may be trapped, etc.).

Various attempts are now being made to include dynamical effects. Progress along these lines is based on the familiar procedure of: 1) choosing the degrees of freedom, 2) formulating the equations of motion (inertias, and forces both conservative and non-conservative), 3) performing the (classical or quantum mechanical) calculations for determining the dynamical evolution of the system, and 4) comparing the results with experiment, after which one re-cycles through from the beginning as new and previously unexplained phenomena are observed.

II. DEGREES OF FREEDOM

The most ambitious calculations being undertaken [4] seek to describe the collision behavior by numerically following the time evolution of a set of fluid elements initially distributed over a grid so as to represent the incoming ions. Figure 1 shows an example of this kind of calculation, where the mass points are constrained to move according to classical incompressible hydrodynamics under the influence of the Coulomb and nuclear forces and subject to damping in the form of viscosity. Because of the numerical complexity of the problem there are no plans to include compressibility or the effect of angular momentum on the system.

Substantial simplification is introduced if a parametrization like the one shown in fig. 2 is chosen for representing the nuclear density distributions [5]. One seeks to employ a multi-dimensional family of shapes that is flexible enough to represent the natural dynamical evolution of the system but has as few parameters as possible. It has often been stressed that at least three degrees of freedom are absolutely essential if the parametrization is to be generally applicable [6-7]. These are: 1) a separation or elongation coordinate, 2) a necking or fragment distortion coordinate, and 3) a mass asymmetry coordinate. In addition to the shape, other degrees of freedom may be important under certain circumstances. For example, it may be necessary to allow the surface diffuseness to vary [8] when calculating the adiabatic nucleus-nucleus interaction potential because there is a tendency for the surfaces to reach out toward each other as the nuclei come together. On the other hand it may be desirable to include compressibility [9-11] as a degree of freedom in highly non-adiabatic situations. It may even be useful to include the degrees of freedom associated with collective giant resonances of various types [9,12].

The ultimate simplification occurs if the nuclear density distributions are simply "frozen" in their original form and are constrained to remain unchanged during the collision. This severe limitation on the degrees of freedom allowed (only the distance between the nuclei and their angular orientation need be considered) drastically restricts the range of applicability of the model. None the less, most of the semi-classical calculations of heavy-ion reactions have

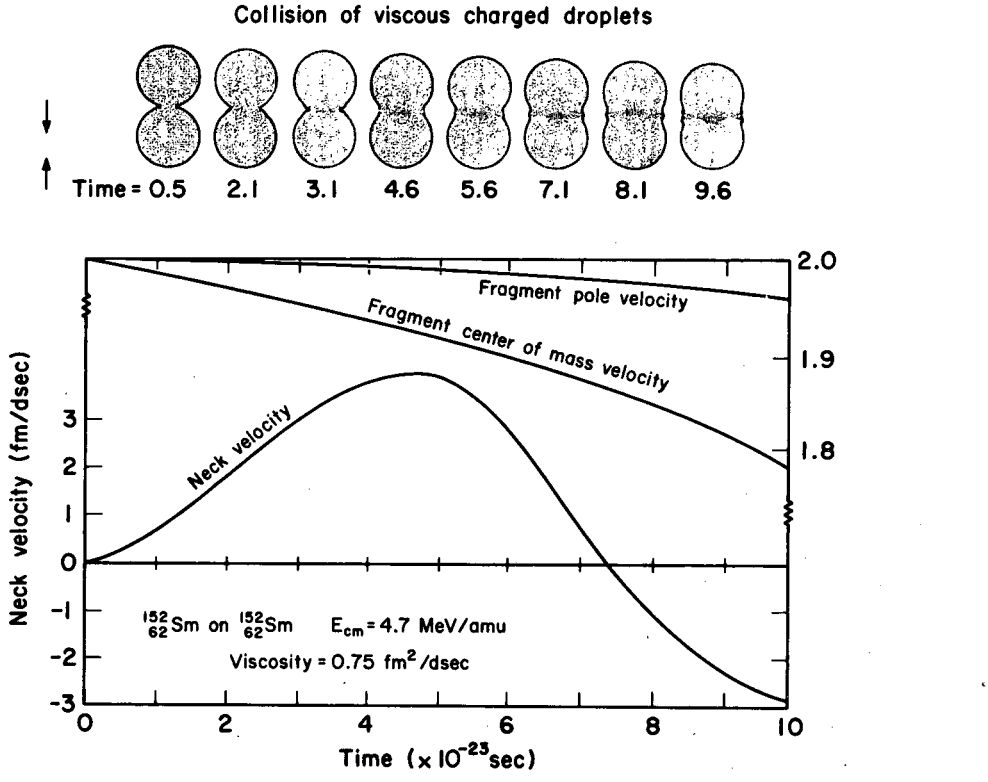

Fig. 1. The result of a numerical study [4] of the dynamic evolution of two uniformly charged liquid drops (with surface tension) is shown for a short time after their initial collision. The parameters have been chosen so that both drops will represent the nucleus ^{152}Sm.

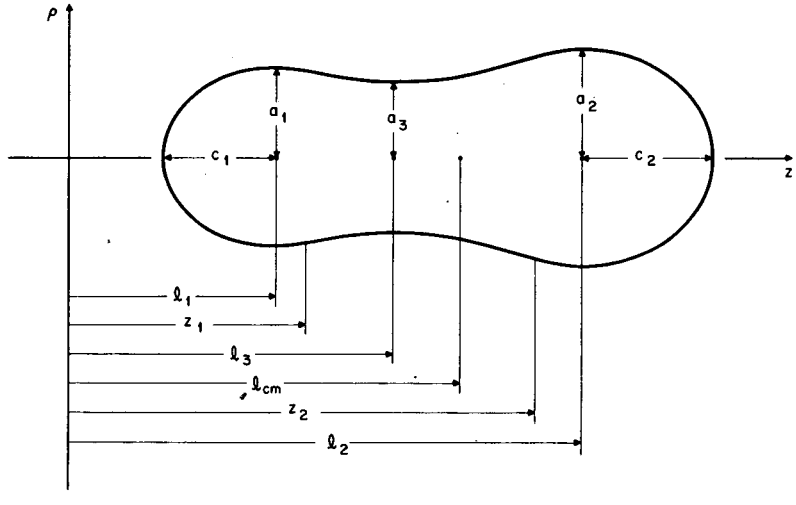

Fig. 2. An illustration of a shape described by three smoothly joined portions of quadratic surfaces of revolution [5]. Each surface is specified by the position ℓ_i of its center, its transverse semiaxis a_i and its semisymmetry axis c_i (the quantity c_3 is imaginary for this shape and hence not shown). The middle hyperboloid of revolution joins smoothly with the two end spheroids at z_1 and z_2. The location ℓ_{cm} of the center of mass of the drop is also shown.

employed this model because of its tractability. The scope at the model is generally tested against the experimental results and other degrees of freedom are sometimes introduced as perturbations to explain some particular result.

III. FROZEN DENSITY DISTRIBUTIONS

Once the distance between the nuclei and their orientations have been chosen as the only degrees of freedom to be treated explicitly (by freezing the densities), the next step is to formulate the equations of motion. Classical mechanics often applies and the inertial parameters are often taken to be the reduced mass of the system and the rigid body moments of inertia. For both the conservative and non-conservative forces that act a wide variety of somewhat similar alternatives have been proposed [13-19].

A. The One-Dimensional Nucleus-Nucleus Potential

Coulomb forces (and sometimes nuclear forces as well) are occasionally considered with respect to the angular degrees of freedom [17,18], but most of the simple calculations that have been done only consider the monopole part of the nucleus-nucleus force and the corresponding potential, which is a function of the distance between the nuclei. These potentials have been chosen in many ways; 1) as simple Woods-Saxon optical model wells with adjustable parameters [20], 2) as the potential generated by folding together the density distribution of the projectile with the single nucleon optical potential of the target [14, 16-19], and 3) as the potential generated by folding a two nucleon potential into the projectile and target density distributions [15,21-23]. For this last type of potential a simple two-parameter Gaussian or Yukawa can be used or one can introduce nuclear saturation by choosing an interaction strength that is density dependent or dependent upon the relative two-body momenta. In addition one can think of the calculation as being performed in the "sudden approximation", where the densities are truly frozen, or in the "adiabatic approximation", where the density distributions are allowed to adjust in some way so as to conserve total volume as the nuclei begin to overlap.

Partly because these approaches are all so similar we haven't strict criteria for choosing between them. However, there are some purely geometrical considerations that one should be aware of and one unifying principle that would greatly simplify these calculations if it were more widely employed.

1. Geometrical Considerations

The error most commonly made in these calculations is to assume that some radial location (such as the half density point or the optical potential half value point) is strictly proportional to $A^{1/3}$. The principle of nuclear saturation, which forms the basis for such assumptions, should be more closely adhered to. It is based on the observation that the bulk density in the central region of nuclei throughout the periodic table is nearly constant. If this is the case then the equivalent sharp radius R is proportional to $A^{1/3}$. For a spherical density distribution with a diffuse surface, purely geometrical considerations [24] govern the relationship between this quantity and the location of the point at which the density has half its central value or 10% of its central value e.g.,

$$R_{50\%} = R\,[1-(b/R)^2 + \cdots] \quad , \qquad (1)$$

$$R_{10\%} = R_{1/2} + a \quad ,$$

where b is a measure of the surface diffuseness whose experimental value is $\sim$ 1 fm, and a is simply the distance between the 50% and 10% points in the diffuse nuclear surface. It would be inappropriate to insist that quantities like these should be strictly proportional to $A^{1/3}$ and then vary the central densities of nuclei in such a way as to bring this about [16,17].

In a similar way, misleading results can be obtained if the half-value point of the single particle optical potential is assumed to be proportional to $A^{1/3}$ rather than relating its location to the density distribution of the nucleus it is supposed to represent. For example, if any expression like eq. (1) is used for the half-value radius of the density [14],

$$R^{\rho}_{1/2} = 1.12\ A^{1/3} - 0.86\ A^{-1/3} \quad , \tag{2}$$

and the half-value radius of the potential is taken to be,

$$R^{V}_{1/2} = 1.25\ A^{1/3} \quad , \tag{3}$$

then the nucleus-nucleus potential generated by folding the projectile density into the target potential is clearly incorrect when one moves away from the central region of the periodic table. If this prescription is applied, then the solid line in fig. 3 represents the distance between the target and projectile half density points (if they both have the same A value) when the projectile half density radius just touches the target half potential radius. If the physically more reasonable assumption is made, that the geometrical properties of the optical potential are related to the density distribution of the nucleus it represents by an expression such as,

$$R^{V}_{1/2} = R^{\rho}_{1/2} + 0.82 - 0.56/R^{\rho}_{1/2} \quad , \tag{4}$$

then the dashed line results [25]. While both these approaches give approximately the same results for nuclei in the middle of the periodic table, only eq. (4) provides a reliable way to extrapolate away from this region.

Nucleus-nucleus potentials generated by folding a two-body force into the target and projectile density distributions are free of the problems cited above so long as the densities are suitably chosen. Furthermore a theorem exists that can greatly simplify such calculations.

2. Proximity Force Theorem

The potential between various sizes of target and projectile interacting via a two-body force can be expressed in terms of a single universal function which is easily obtained [23]. This is because of the fact that,

> "The <u>force</u> between rigid gently curved surfaces is proportional to the <u>potential</u> per unit area between flat surfaces."

For frozen, spherical density distributions the force between two nuclei as a fucntion of the distance s between their surfaces is given by,

$$F(s) = 2\pi\ R_r\ e(s) \quad , \tag{5}$$

where the "reduced radius" $R_r = R_1R_2/(R_1+R_2)$ and e(s) is the potential energy per unit area, as a function of the separation s of two flat surfaces interacting via the appropriate two-body force. This expression applies (so long as R_1 and R_2 are large compared to the range of the force) to any target and projectile combination.

Recognition that the touching of two flat surfaces results in a potential energy gain per unit area equal to twice the surface energy coeffient γ imposes the important constraint that

$$e(o) = -2\gamma \quad . \tag{6}$$

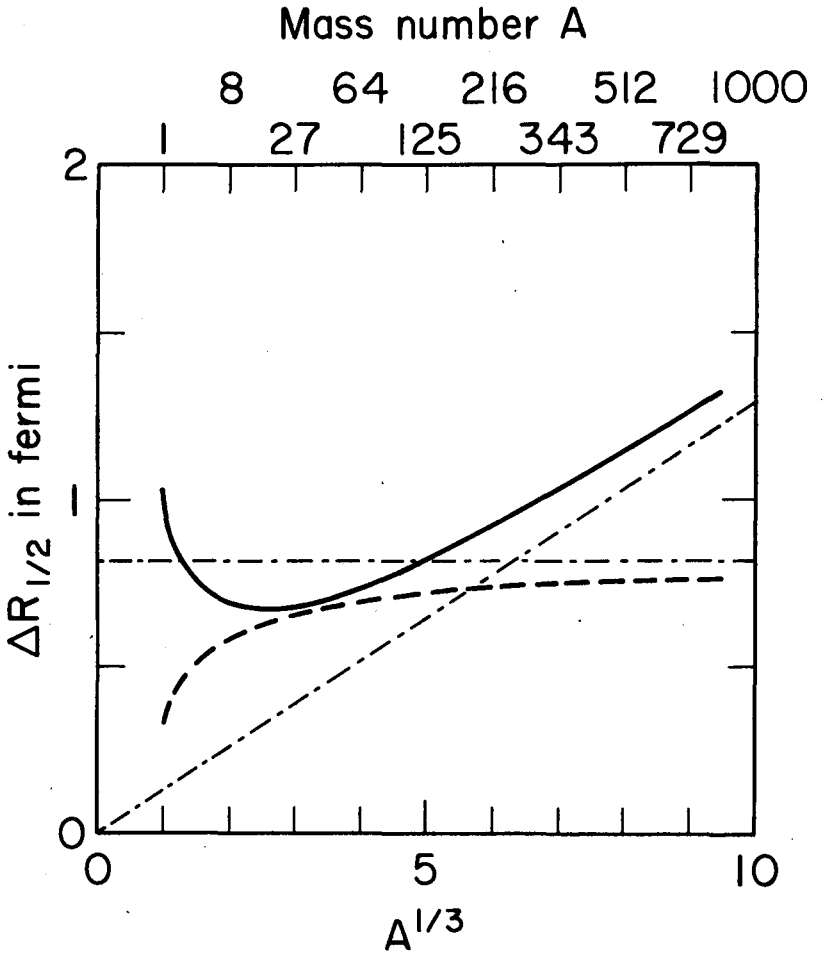

Fig. 3. The distance between half-density points of two identical nuclei is plotted against their mass number when they are separated so that the half-density point of one coincides with the half-potential point of the other. The solid line corresponds to the choice of parameters in ref. [14] and the dashed line to the choice in ref. [25].

In addition the force between two flat surfaces should become repulsive, because of nuclear saturation, as the density distributions begin to overlap. This means that the maximum potential energy gain between two flat surfaces occurs when they touch, and hence the maximum force between two finite nuclei occurs [13] when s=0, and it has the value

$$F_{max} = F(o) = -4\pi R_r \gamma \quad . \tag{7}$$

Figure 4 shows how the function e(s) appears for the particular choice of a saturating, momentum dependent, two-body interaction [22]. The lower part of the figure is a plot of the function f(s) which is defined by the expression,

$$f(s) = \int_s^\infty e(\acute{s})\, d\acute{s} \quad . \tag{8}$$

The interaction potential between target and projectile can be written in terms of this universal function as

$$V(s) = 2\pi R_r f(s) \quad . \tag{9}$$

B. Static and Dynamic Considerations

Much of the work that is based on frozen density distributions and the corresponding one-dimensional nucleus-nucleus potential consists of attempts to find correlations between the cross-sections for various processes and certain static features of the interaction [13-19]. Figure 5 shows a typical example of the nucleus-nucleus potential for the case of $^{40}Ar + ^{109}Ag$. The curves show the combined Coulomb, nuclear (according to eq. (9) and a function f(s) similar to the one in fig. 4) and centrifugal potentials for various values of the incident angular momentum. At a radial distance of about 9.6 fm, which is indicated by a vertical dashed line, the equivalent sharp surfaces of these two nuclei just touch. The range of the nuclear interaction potential (see fig. 4) is such that its effect should be just barely detectable about 3 fm further out at the radial location indicated by the vertical dot-dashed line. The total reaction cross-section is expected to be proportional to the probability for reaching this outer radius, and the cross-section for massive transfers and compound nucleus formation is expected to correspond to reaching an inner radius where absorption begins to take place (for purposes of illustration we take this to be the point of touching).

Simple energy and angular momentum conservation considerations give rise to an expression for the energy dependence of these cross sections which is

$$\sigma_R(E) = \pi R^2 \left(1 - \frac{V(R)}{E}\right) \quad , \tag{10}$$

where V(R) is the sum of the Coulomb and nuclear potentials at the radius R. The cross-section for reaching the outer radius in fig. 5 predicted by eq. (10) is given by a dot-dashed line in fig. 6. It has its threshold at about 97 MeV where the incoming projectile is first able to reach the point labeled C in fig. 5. The dashed curve and its solid extension in fig. 6 represents the cross-section for reaching the inner radius where solid contact takes place. It is easy to see that the first part of this curve is misleading. Its threshold at about 80 MeV corresponds to reaching the point labeled A which is inaccessable because of the potential barrier. The actual cross-section for obtaining solid contact has its threshold at 103 MeV where the incoming projectile first begins to surmount the barrier at point B. The solid line originating at point B that arcs upward to join the vertical dashed line in fig. 5 is the locus of those radii that must be reached in order for solid contact to take place. The solid curve in fig. 6 that joins the dashed curve at a point corresponding to the disappearance of the hollow in the potential energy curve (labeled D in fig. 5) corresponds to the actual cross-section for obtaining solid contact. It is clear

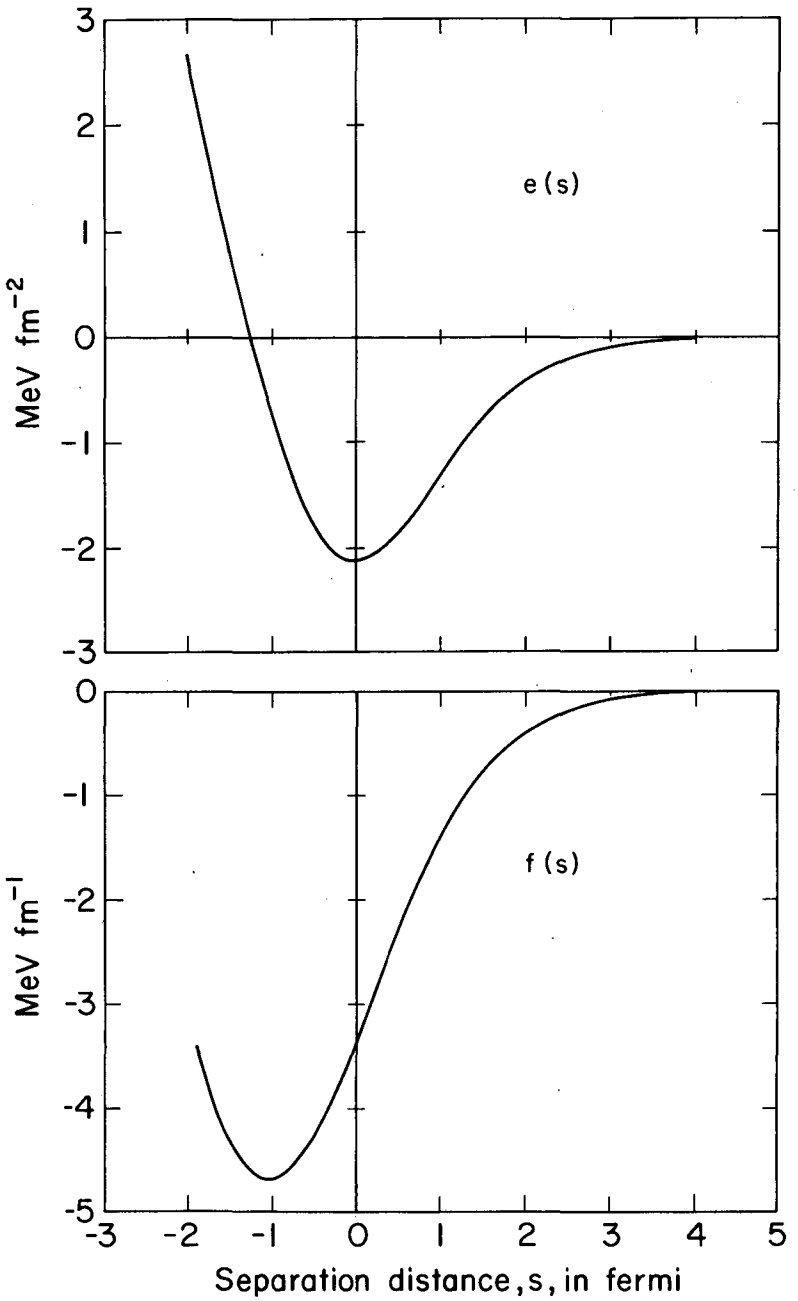

Fig. 4. The upper curve represents the potential energy per unit area of two semi-infinite, diffuse, nuclear density distributions as a function of their separation [22]. The lower curve (which is the integral of the upper one) gives the dependence of the total interaction energy of two finite nuclei on the separation between their surfaces.

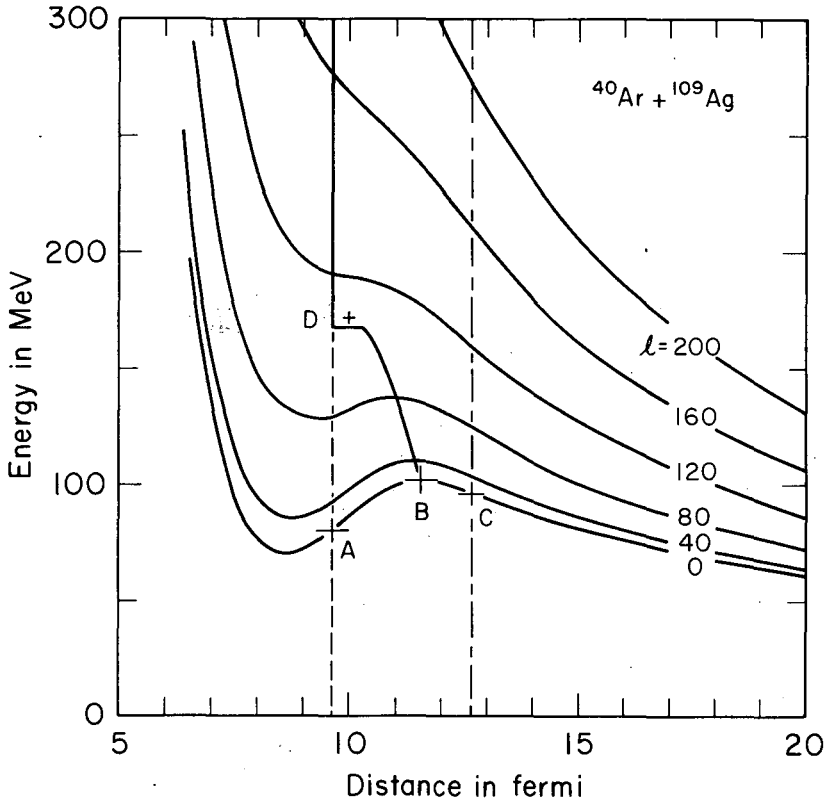

Fig. 5. The total potential energy (Coulomb, nuclear and centrifical) of the nuclear system $^{40}Ar + ^{109}Ag$ is plotted against the distance between their centers, for different values of the angular momentum. The vertical dot-dashed line corresponds to the distance where the nuclear force is first expected to exert its influence. The vertical dashed line corresponds to the point where the equivalent sharp surfaces of the two nuclei come into contact.

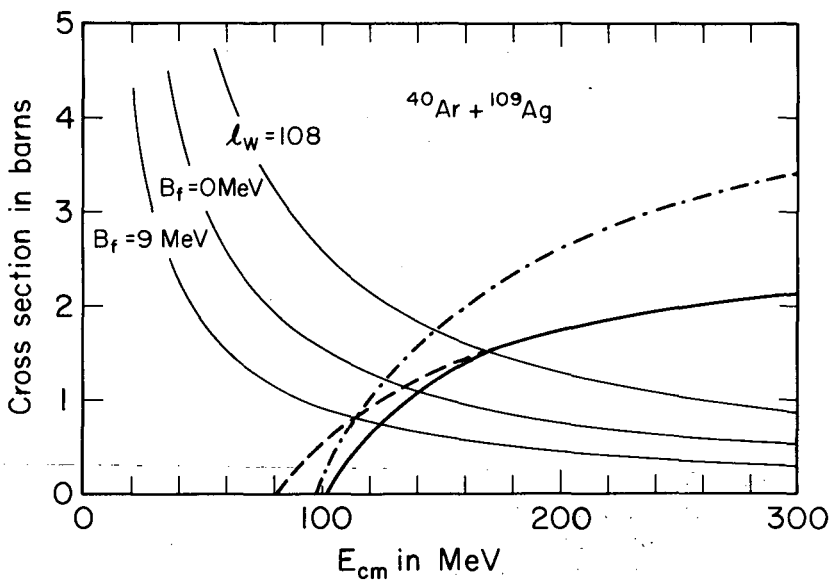

Fig. 6. The cross-sections for reaching certain radial separations are plotted against the center of mass energy for the same system as is treated in fig. 5. The solid line that merges with the dashed line is the cross-section for solid contact, the dot-dashed line the cross-section for just barely touching. The line labeled $\ell_w = 108$ the limit imposed by the vanishing of the hollow in the two-body potential due to increasing angular momentum. The lines labeled $B_f = 0$ and 9 MeV are the angular momentum imposed limits to compound nucleus formation corresponding to the lowering of the fission barrier either to zero or the neutron binding energy [40].

from these considerations that misleading results may be obtained for the values of the solid contact radius and the potential at that point if they are determined by fitting a function like eq. (10) to the beginning part of this curve [26,27].

1. Trapping

The gross features of heavy-ion elastic scattering are described rather well by assuming that all the incoming projectiles whose energy and angular momentum permit them to pass over (or penetrate through) the barrier in the potential energy are removed from the entrance channel. For light projectiles and energies not too far above the Coulomb barrier most of the nuclei which pass over the barrier actually combine with the target to form a compound nucleus. For these systems the hollow in the one-dimensional potential energy disappears when the incident angular momentum is too large, and the compound nucleus cross-section seems to be limited by the critical angular momentum [13] at which this occurs. The curve labeled ℓ_w in fig. 6 (which passes close to the point where the solid and dashed lines come together) shows the sort of limitation such a critical angular momentum would place on the absorption cross-section. Substantial deviations from this simple approach have been observed for more massive projectiles and higher energies [15,29], and even for lighter systems there are dynamical considerations, such as those illustrated in fig. 7, that show the model to have certain weaknesses. An alternative description in terms of a strong absorption radius, $R = 1 \cdot (A_1^{1/3} + A_2^{1/3})$, has been shown to give good agreement for a wide range of experiments [15].

The upper right portion of fig. 7 is meant to represent the idea that all incident nuclei that pass over the barrier are expected to drop into the hollow and be absorbed [23]. However, when two nuclei overlap sufficiently for absorption to take place the projectile tends to set the target spinning which reduces the orbital angular momentum and the system sees a potential corresponding to a smaller value of L. The upper left illustration shows how this might allow the projectile to escape even though the energy loss in the radial motion would have been sufficient to cause trapping in the original well.

The lower right illustration represents the idea that absorption can not take place if there is no hollow in the potential energy. The lower left part of the figure shows how the loss of orbital angular momentum might result in a potential having a barrier and the corresponding loss in radial energy could lead to trapping.

2. Absorption

Even though absorption (and hence compound nucleus formation) are almost synonymous with trapping for lighter mass projectiles, substantial difficulties arise when the mass asymmetry between target and projectile is reduced. We have to extend our thinking to the other essential degrees of freedom if we want to understand the origin of these difficulties.

Figure 8, which includes a "necking" degree of freedom $\tilde{\alpha}_4$ as well as a separation coordinate $\tilde{\alpha}_2$, serves to remind us that the two fragment valley of two colliding nuclei does not lead directly to the ground state configuration of the compound system [7,28]. Indeed, if the trapping configuration corresponds to a point in this two-dimensional space like to one labeled A then no hope of compound nucleus formation exists unless enough additional energy is added to drive the system over the intervening ridge toward the spherical ground state at point H. Even then a compound nucleus might not result because the energy in the collective degrees of freedom would be sufficient to bring the system out over the fission barrier at point S.

There is a one-dimensional way of estimating whether or not two nuclei in contact are likely to diffuse down into a compound nucleus. This can be done by calculating the "compactness" of the contact configuration to see if it lies inside or outside that of the fission barrier. In fig. 9 the potential energies of two heavy-ion systems leading to the same compound nucleus ^{248}Fm are plotted

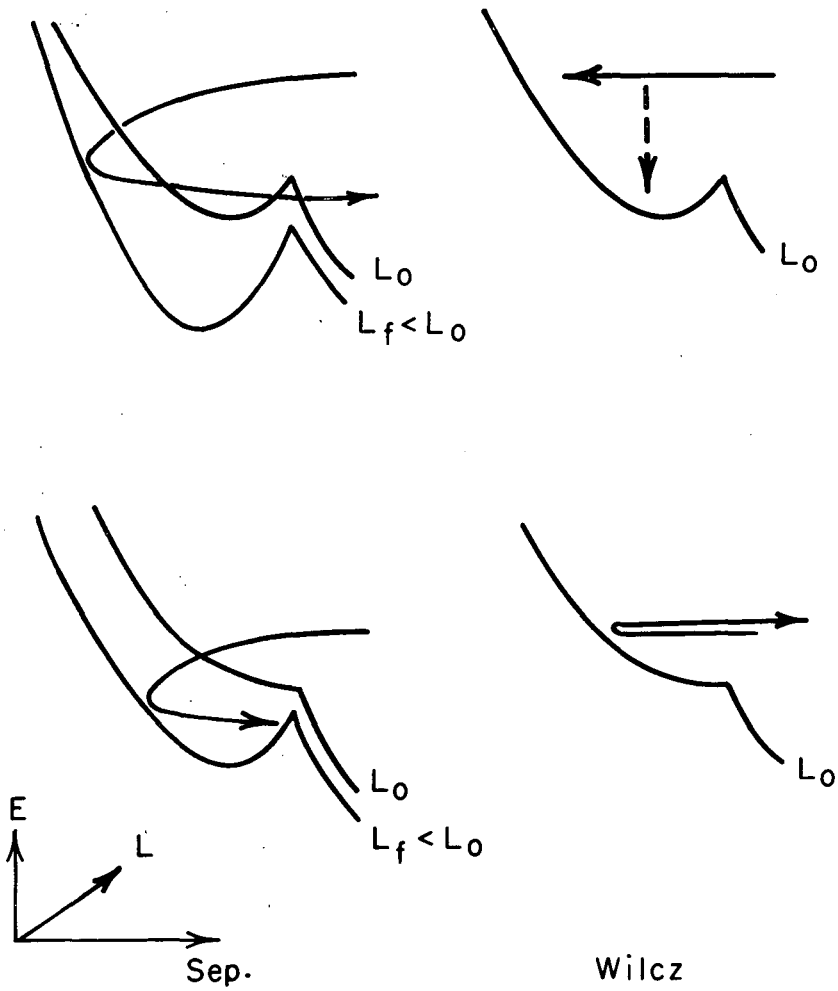

Fig. 7. A schematic representation of the capture process in heavy-ion scattering to illustrate some of the consequences of friction during the collision [23]. The separate parts of the figure are discussed in the text.

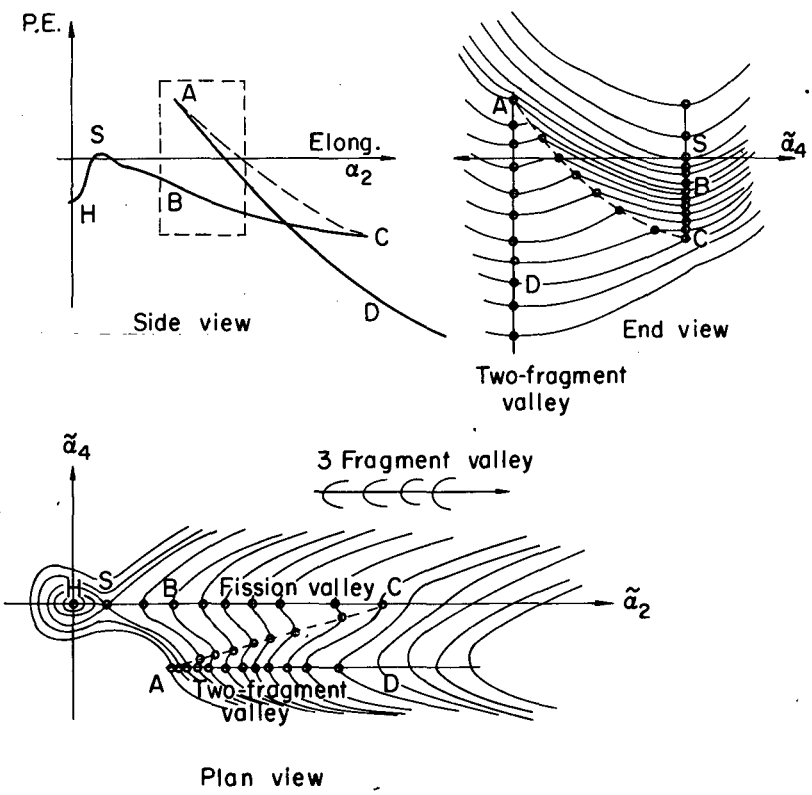

Fig. 8. Schematic energy contour diagrams of the two-fragment valley and the fission valley [7].

against their quadrupole moment [23] (as a measure of compactness). The fission barrier of ^{248}Fm is also shown, and we see that the compactness of the stuck configuration of $^{232}U + ^{16}O$ (which is known to form this compound nucleus) is almost the same as that of the ^{248}Fm ground state. The system $^{208}Pb + ^{40}Ar$ (which does not readily form the compound nucleus) has a stuck configuration whose compactness lies much further out on the fission barrier. This particular figure only applies to the case of L=0. The introduction of angular momentum not only reduces the chances of compound nucleus formation by moving the minimum in the nucleus-nucleus potential outward (or washing it out completely) but it also reduces the barrier height of the compound system.

Any attempt to determine the effectiveness of additional energy over the Coulomb barrier in driving the system toward a spherical configuration must include a dynamical treatment of the relevant degrees of freedom like that shown in fig. 10 [30]. The calculations on which this figure is based employ the three symmetric degrees of freedom of the shape parametrization shown in fig. 2. They assume non-viscous, irrotational, hydrodynamic flow and are restricted to the case of L=0. In spite of all these limitations the figure dramatically illustrates the fact that the system must have an energy of 50 or 100 MeV over the Coulomb barrier before it even begins to move in the direction of compound nucleus formation.

Figure 11 shows how the addition of angular momentum also acts in a way so as to reduce the probability of absorption for heavier projectiles [23]. In this figure x is the usual fissility parameter (the Coulomb energy of the compound system in units of twice the surface energy) and y is the rotational energy of the system in units of the surface energy. The quantity u is the mass asymmetry of the target, projectile combination. The contact configuration will tend toward amalgamation if the corresponding point in the x,u plane lies below the appropriate y-curve. If the point lies above this curve then the target and projectile will be repelled.

Even for L=0, simple surface energy and Coulomb energy considerations act to reduce the tendency toward compound nucleus formation when heavier projectiles are used, or attempts are made to form more massive final products. Figure 12 is a plot of the relative potential of touching spheres as a function of mass asymmetry for two different systems [31]. Even for the lighter system we see that the driving force toward absorption becomes weaker the more symmetric is the target projectile combination. For the heavier system the situation is even more dramatic. If the initial contact configuration is not sufficiently asymmetric then the driving force in the asymmetry degree of freedom pushes the system toward two equal spheres in contact, and subsequent separation in a fission like mode.

IV. NEW PHENOMENA

The considerations of the previous section make it abundantly clear that when heavier projectiles are used compound nucleus formation is no longer expected to be the primary result of bringing two nuclei into contact. A host of new phenomena are expected to arise because the time constants for various types of collective motion (rotation, vibration, neck healing, mass asymmetry, etc.) are roughly comparable [32]. Of course this is also true for lighter projectiles, but the interchange of energy among the various collective degrees of freedom and the damping into intrinsic states is not experimentally observable because the end result of the collision is usually a compound nucleus. The important difference is that systems formed with heavier projectiles are expected to re-disintegrate giving us the opportunity to observe the consequences of interaction of the various degrees of freedom during the collision.

A number of dynamical calculations are being attempted within the macroscopic, semi-classical approach [9,23,28,30,31,33-35] as an aid to understanding the wealth of new phenomena being observed. Some are simple one-dimensional models with damping but others are considerably more ambitious.

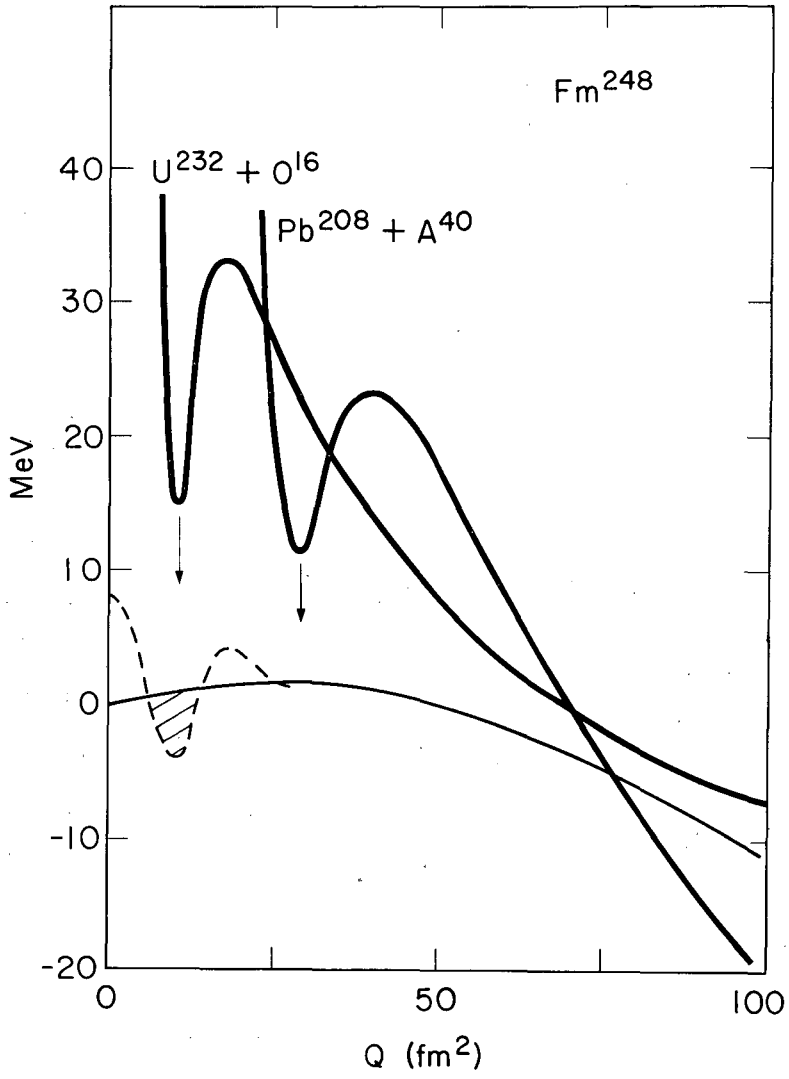

Fig. 9. The nucleus-nucleus potential energy as two nuclei are brought together is plotted against the quadrupole moment of the system for two different combinations of target and projectile leading to the same compound nucleus. The fission barrier of the ground state of the compound system is also shown.

Fig. 10. Calculated dynamical paths [30] for the system $^{150}Nd + {}^{150}Nd \rightarrow {}^{300}120$. The nuclear viscosity is zero, and the finite range of the nuclear force is taken into account in calculating the nuclear macroscopic energy. Each path corresponds to starting the system from the contact point with the indicated amount of center-of-mass kinetic energy relative to this point (in units of MeV). Because of deficiencies in the shape parametrization the dynamical calculations break down at the points indicated by the arrowheads.

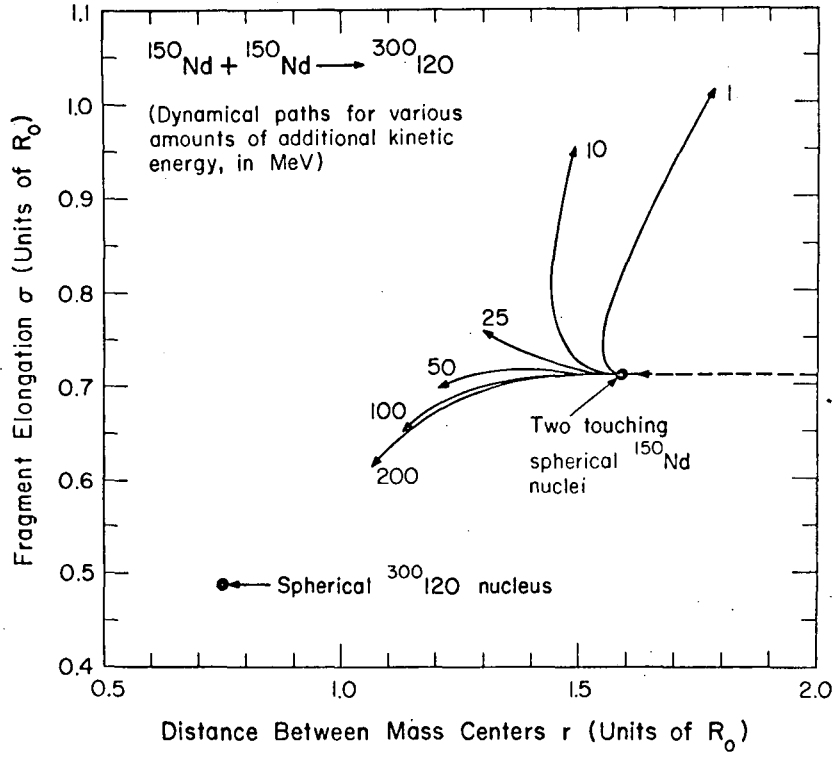

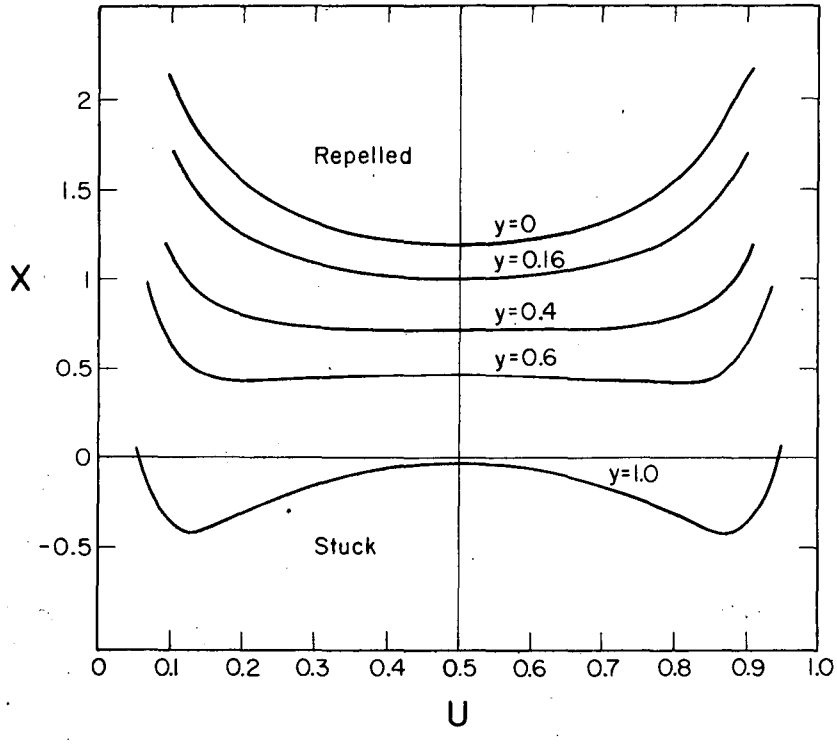

Fig. 11. This figure shows how the ability of the nuclear forces to hold two nuclei together depends on angular momentum [23]. The quantity X is the usual "fissility parameter" which is the ratio of the Coulomb energy of the compound system to twice the surface energy. (Negative values of this variable correspond a Coulomb like interaction which is attractive rather than repulsive, i.e., gravitation. Large negative values of X are relevant for stability problems of astrophysical interest.) The quantity U is the mass asymmetry $[m_1/(M_1 + M_2)]$ of the system, and y is the ratio of the rotational energy to the surface energy of the compound system. If the (X,U) point describing the system lies above the corresponding y curve the nuclei will tend to be driven apart.

Fig. 12. Illustrates how the energy of two nuclei in contact depends on the mass asymmetry of the system and on the particular compound nucleus they would produce if they combined [31].

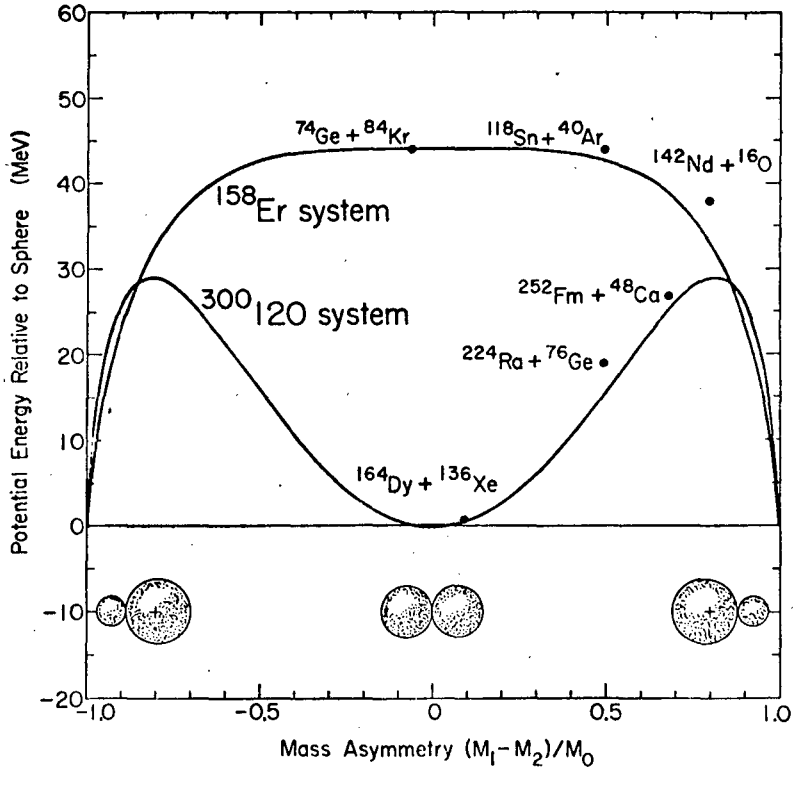

A. Viscosity

In the scattering of ^{40}Ar on ^{232}Th at a center of mass energy of 331 MeV the emerging K nuclei (one proton and perhaps a few neutrons are picked up from the target) have the energy and angle distributions shown in fig. 13 [36]. Figure 14 shows how this kind of distribution might be generated by viscous forces acting on projectiles that pass close to the nucleus. Trajectories corresponding to impact parameters smaller than those that lead to grazing collisions will not only be slowed down but will also be deflected forward to smaller angles. Figure 15 illustrates the results of a simplified dynamical calculation of this process [23]. It shows how the experimental results can be used to infer the strength of the frictional forces acting between nuclei.

B. Mass Dispersion

Almost all of the experiments being conducted with more massive projectiles result in products whose masses are widely distributed over the periodic table. The actual distribution that results may consist of a number of different components with separate origins corresponding to different ranges for the initial angular momentum of the system.

Figure 16 shows the range of nuclei that result from the collision of ^{40}Ar and $^{107-109}Ag$ at 288 MeV [32]. The yield is seen to drop off as one moves away from the Z of the projectile toward lighter nuclei. In this particular case the cross-sections for the production of all these different nuclei peak in the forward direction, implying a time constant for the mass transfer that is short compared to that for the rotation of the system. One interesting aspect of this particular experiment is that the kinetic energy of all of these products (regardless of mass or scattering angle) corresponds to the Coulomb repulsion between them and their corresponding partner in a two-body breakup (see fig. 17, [32]). The energy of the incident projectile seems to have been completely absorbed.

One of the most fascinating mass distributions I have seen so far was obtained by radio-chemical means for the scattering of ^{84}Kr on ^{238}U [37]. In fig. 18 we see that there are two sharp peaks corresponding to stripping and pickup reactions, and the double peaks (which contain about 200 mb of cross-section) arise from the asymmetric fission of some of the target nuclei after these collisions. There is also a broad peak centered around the projectile mass that corresponds to a distinctly different process involving massive transfers. The rather broad peak just beside this one results from the fission of the more massive partner resulting from these transfers. In addition, a broad peak is observed that seems to correspond to compound (or at least composite) nucleus formation. The peak at $A \approx 195$ is completely unexplained.

C. Focusing

When the periods for vibration (or neck healing) and rotation become comparable certain types of focusing can take place. Figure 19 is the angular distribution of light products (assumed to be similar to the ^{84}Kr projectile) scattered from ^{209}Bi having energies distinctly lower than the bombarding energy [38]. These products seem to correspond to collisions where radial motion of the incoming projectile is completely stopped and the system rotates with the incident angular momentum while some other collective vibration (such as neck healing and reforming) takes place. The vibration and rotation rates for different incident angular momentum seem to be correlated in such a way as to focus all the products into a rather narrow range of forward angles.

Exactly the same peak has also been seen at the somewhat higher bombarding energy of 605 MeV [39]. In that case it occurs quite a bit further forward, at 52° in the center-of-mass. The broad mass peak centered around Kr in fig. 18 probably corresponds to these nuclei that are focused at forward angles and whose kinetic energy is just that of Coulomb repulsion. If this is the case, the width of the peak in the mass distribution probably depends on the time it takes for the collective motions that cause focusing to take place. It should be

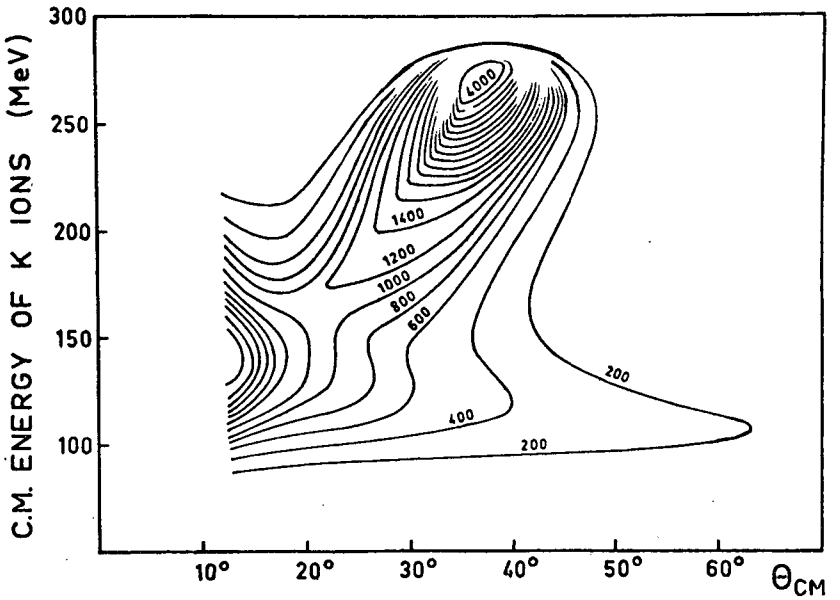

Fig. 13. The yield contours for the reaction $^{232}Th(^{40}Ar,K)$, E_{lab} = 388 MeV are plotted against the center-of-mass energy and deflection angle [36].

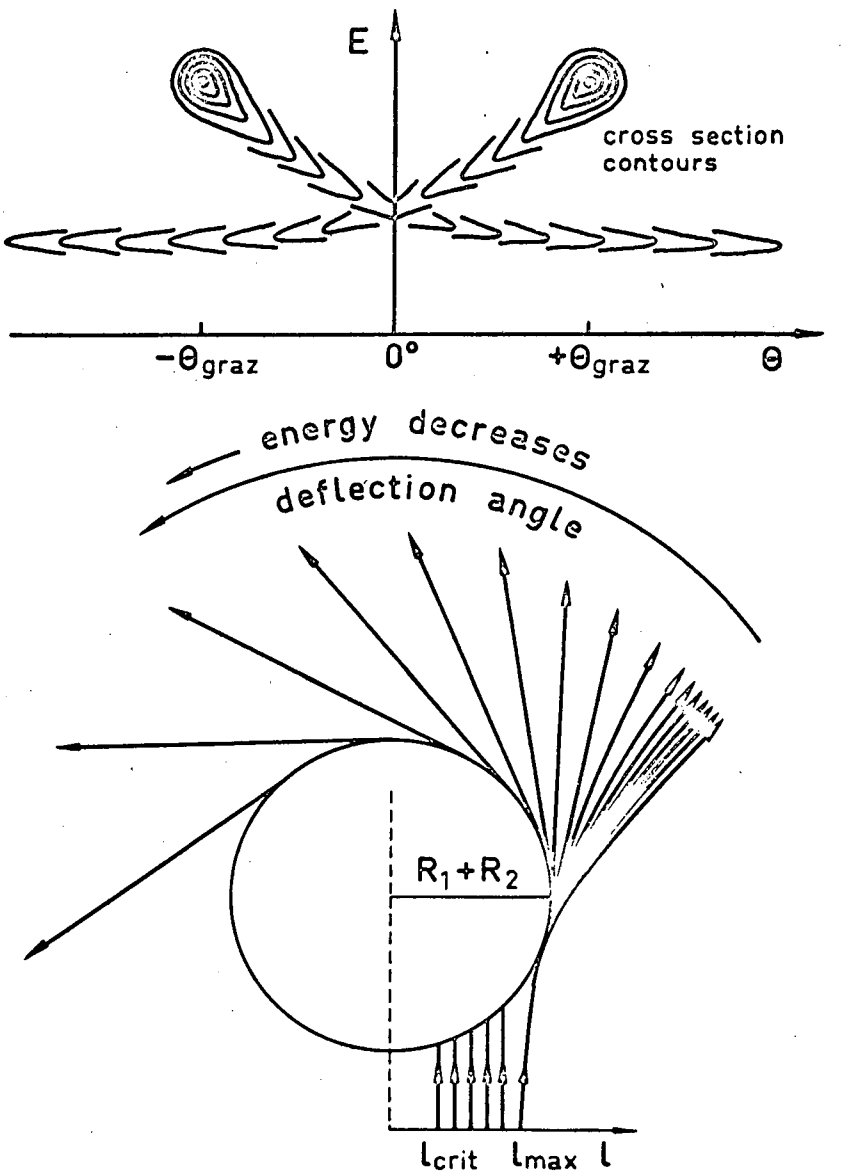

Fig. 14. This figure proposes a mechanism to explain the yield curves in fig. 13. It is proposed that projectiles with small impact parameters may be both swept around to smaller deflection angles by the nuclear forces and also slowed down by friction during the collision [36].

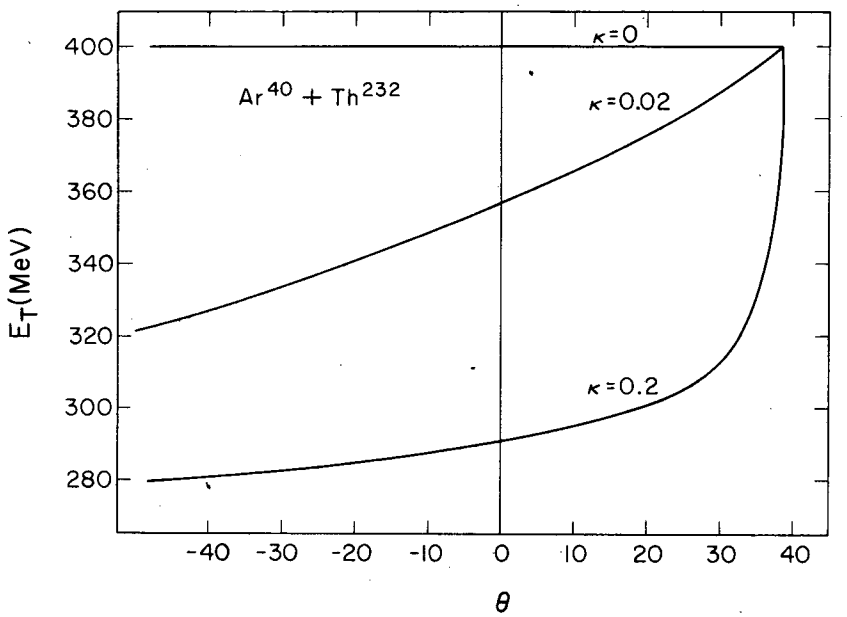

Fig. 15. The results of an actual calculation [23] of the dependence of the energy on deflection angle are shown for three different values of the friction coefficient.

Fig. 16. The differential cross-section as a function of the projectile change is shown for a number of different scattering angles [32].

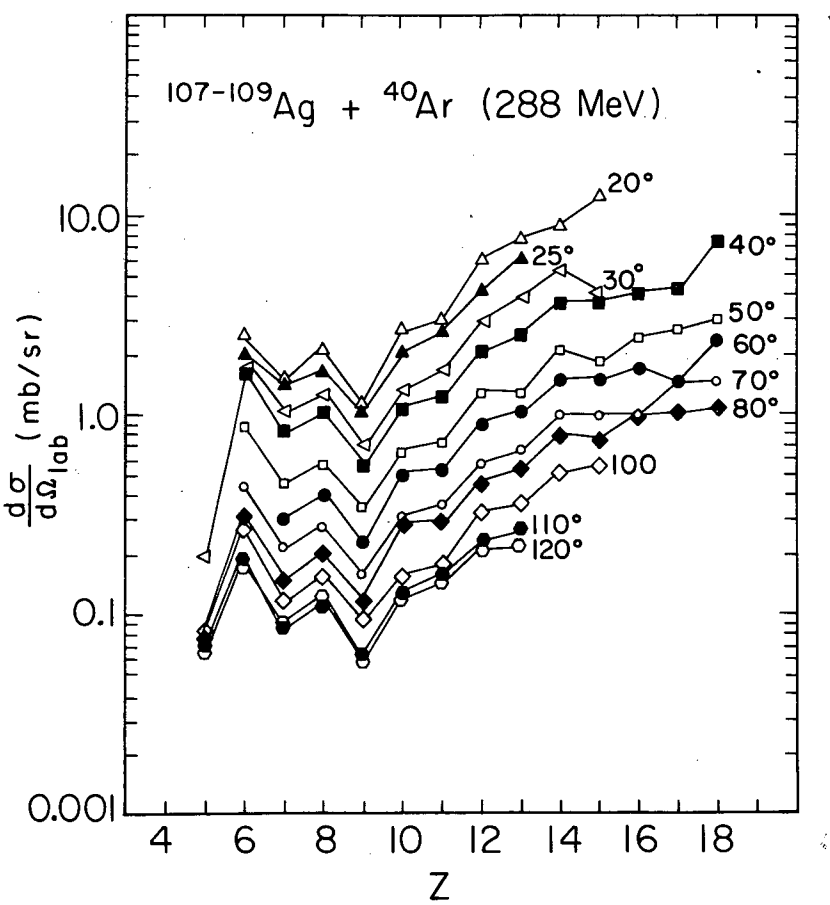

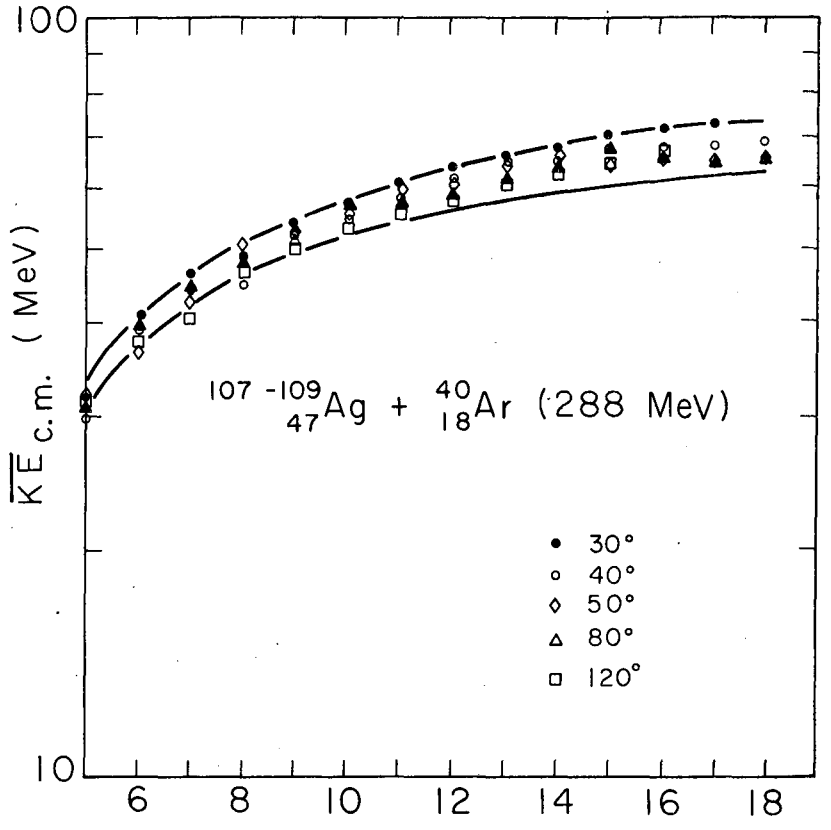

Fig. 17. The center-of-mass kinetic energy of a range of products arising from the indicated reaction is plotted against the Z of the product. The solid lines are two estimates of the energy these products would have on the basis of pure Coulomb repulsion. The result is seen to be independent of scattering angle [32].

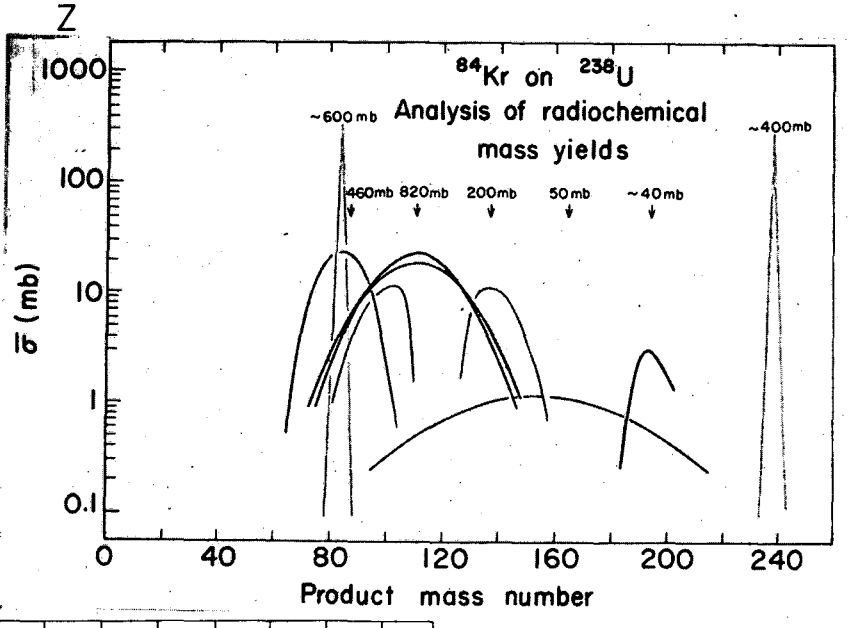

Fig. 18. Analysis of radiochemical mass yields from the thick target bombardment of ^{238}U with ^{84}Kr and 605 MeV. The various components of the yield that can be separately identified are discussed in the text [37].

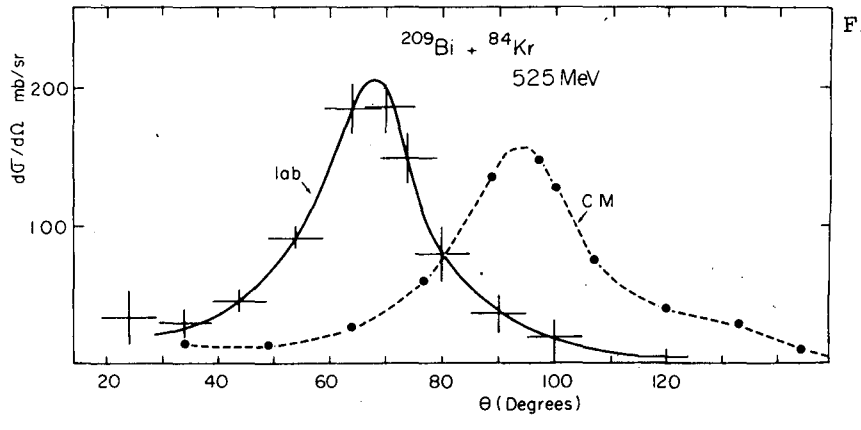

Fig. 19. This figure shows the angular distribution of products from the indicated reaction that have an energy much lower than the incident energy. The energy observed is approximately that of Coulomb repulsion from a configuration of contact with the target nucleus [38].

possible to determine the time constants for many of these degrees of freedom by varying the experimental conditions.

V. SUMMARY

Some reasons were given for the sudden surge of interest in the macroscopic approach to heavy-ion reactions. Then a number of different ways were mentioned for dealing with the many degrees of freedom inherent to the problem. The discussion was then carried on largely in the framework of the one-dimensional models that have been most heavily treated. Various geometrical considerations that bear on these models were presented and some of the applications to reaction and compound nucleus formation cross sections were mentioned. Then a number of reasons were given for the difficulty encountered in forming a compound system when heavier projectiles are used and it was pointed out that a whole host of new phenomena are expected to occur. Some of these new effects are already being observed. They promise to provide information on nuclear viscous (or damping) forces, on various nuclear time constants, and on the nature of the mechanical and hydrodynamical behavior of the smallest (clearly composite) system known to man.

ACKNOWLEDGMENTS

The author wishes to acknowledge the substantial contributions of his colleagues, in particular W. J. Swiatecki, C. F. Tsang, and N. K. Glendenning. He is indebted to many others for useful discussions and a wealth of material provided prior to publication, those include C. Alonso, J. R. Nix, F. Plasil, L. G. Moretto, V. Viola, J. V. Kratz, H. Gutbrod, and J. Huizenga.

REFERENCES

1. M. Blann, Proceedings of the International Conference on Nuclear Physics, Munich, August 1973, North-Holland Publishing Co.
2. F. Plasil, Paper DB2, American Physical Society Meeting, Washington, D. C., April 1974.
3. A. Fleury and J. M. Alexander, preprint, May 1974.
4. Carol Alonso, private communication.
5. J. R. Nix, Nucl. Phys. A130 (1969) 241.
6. W. J. Swiatecki, Proceedings of the International Conference on Nuclear Reactions Induced by Heavy-Ions, Heidelberg, July 1969, North-Holland Publishing Co.
7. W. J. Swiatecki, Phys. Letters 4C (1972) 326.
8. J. Randrup, contribution to this conference.
9. W. Greiner, Proceedings of the International Conference on Nuclear Reactions Induced by Heavy-Ions, Heidelberg, July 1969, North-Holland Publishing Co., and references there.
10. W. Scheid, H. Müller, and W. Greiner, Phys. Rev. Letters 32 (1974) 741; and contribution to this conference.
11. C. Y. Wong and T. A. Welton, preprint (1974), and contribution to this conference.
12. A. S. Jenson and C. Y. Wong, Phys. Letters 32B (1970) 567.
13. J. Wilczynski, Nucl. Phys. A216 (1973) 386.
14. D. H. E. Gross and H. Kalinowski, Phys. Letters 48B (1974) 302; and contribution to this conference.
15. J. Galin, D. Guerreau, M. Lefort, and X. Tarrago, Phys. Rev. 9C (1974) 1018.
16. D. M. Brink and N. Rowley, Nucl. Phys. A219 (1974) 79.
17. N. Rowley, Nucl. Phys. A219 (1974) 93.
18. C. Y. Wong, Phys. Letters 42B (1972) 186.
19. R. Bass, Phys. Letters 47B (1973) 139, and contribution to this conference.
20. Session IV this conference for example.
21. H. J. Krappe and J. R. Nix, Proceedings of the Third Symposium on the Physics and Chemistry of Fission, Rochester, August 1973.

22. J. Randrup, private communication.
23. W. J. Swiatecki and C. F. Tsang, private communication.
24. W. D. Myers, Nucl. Phys. A204 (1973) 465.
25. W. D. Myers, Nucl. Phys. A145 (1970) 387.
26. H. H. Gutbrod, M. Blann, and W. G. Winn, Nucl. Phys. A213 (1973) 267.
27. D. Glas and U. Mosel, contribution to this conference.
28. A. J. Sierk and J. R. Nix, ibid.
29. J. Huizenga, private communication.
30. A. J. Sierk and J. R. Nix, Proceedings of the Third Symposium on the Physics and Chemistry of Fission, Rochester, August 1973.
31. J. R. Nix, Paper DB1, American Physical Society Meeting, Washington, D. C., April 1974.
32. L. Moretto, Paper DB3, ibid.
33. R. Beck and D. H. E. Gross, Phys. Letters 47B (1973) 143.
34. R. H. Davis, Phys. Rev. C, to be published, and contribution to this conference.
35. J. Bondorf, contribution to this conference.
36. J. Wilczynski, Phys. Letters 47B (1973) 484.
37. J. V. Kratz, A. E. Norris, and G. T. Seaborg, private communication; see also J. V. Kratz, J. O. Liljenzin, A. E. Norris, I. Binder, and G. T. Seaborg, contribution to this conference.
38. F. Hanappe, M. Lefort, C. Ngô, J. Peter, and B. Tamain, Phys. Rev. Letters 32 (1974) 738, and contribution to this conference.
39. K. Wolf, J. Huizenga, J. Unik, V. Viola, J. Birkelund, and H. Freiesleben, private communication.
40. S. Cohen, F. Plasil, and W. J. Swiatecki, Ann. Phys. (NY) 82 (1974) 557.

TECHNICAL INFORMATION DIVISION
LAWRENCE BERKELEY LABORATORY
UNIVERSITY OF CALIFORNIA
BERKELEY, CALIFORNIA 94720